Published in final edited form as:
Cell Host Microbe. 2012 May 17; 11(5): 504–514. doi:10.1016/j.chom.2012.03.005.

Alphaherpesvirus infection disrupts mitochondrial transport in neurons

Tal Kramer[1] and **Lynn W. Enquist**[1,*]
[1]Department of Molecular Biology, Princeton University, Princeton, NJ 08544

SUMMARY

Mitochondria are dynamic organelles that are essential for cellular metabolism but can be functionally disrupted during pathogen infection. In neurons, mitochondria are transported on microtubules via the molecular motors kinesin-1 and dynein and recruited to energy-requiring regions such as synapses. Previous studies showed that proteins from pseudorabies virus (PRV), an alphaherpesvirus, localize to mitochondria and affect mitochondrial function. We show that PRV and herpes simplex virus type 1 (HSV-1) infection of rodent superior cervical ganglion (SCG) neurons disrupts mitochondrial motility and morphology. During PRV infection, glycoprotein B (gB)-dependent fusion events result in electrical coupling of neurons and increased action potential firing rates. Consequently, intracellular [Ca^{2+}] increases and alters mitochondrial dynamics through a mechanism involving the Ca^{2+}-sensitive cellular protein Miro and reduced recruitment of kinesin-1 to mitochondria. This disruption in mitochondrial dynamics is required for efficient growth and spread of PRV, indicating that altered mitochondrial transport enhances alphaherpesvirus pathogenesis and infection.

INTRODUCTION

Mitochondria are essential organelles involved in a variety of cellular and metabolic processes including ATP production, Ca^{2+} homeostasis, and programmed cell death. In neurons, mitochondria are highly dynamic and are targeted to regions of the cell with increased energy demands such as growth cones and synapses (Chang et al., 2006; Li et al., 2004). Disruption of mitochondrial function and dynamics is implicated in a variety of neurodegenerative diseases and neuropathies (Sheng and Cai, 2012). An increasing number of pathogens, including viruses and bacteria, have been shown to directly or indirectly alter mitochondrial function and dynamics (Ohta and Nishiyama, 2011). However, for many of these pathogens, the role of mitochondrial disruption during infection and the subsequent consequences for host cell function remain poorly understood.

The mammalian alphaherpesviruses invade the peripheral and central nervous system of their hosts (Pellett and Roizman, 2007). Well-studied alphaherpesviruses include the human pathogens herpes simplex virus 1 and 2 (HSV-1 and HSV-2), and varicella zoster virus (VZV), as well as the swine pathogen pseudorabies virus (PRV) (Pomeranz et al., 2005). These viruses are pantropic and neuroinvasive. Once in the peripheral or central nervous

*Corresponding Author: Lynn W. Enquist, Princeton University, Department of Molecular Biology, 314 Schultz Laboratory, Princeton, NJ 08544, 609-258-2415 (Office), 609-258-1035 (Fax), lenquist@princeton.edu.

system, infection can spread within chains of synaptically connected neurons. Consequently, HSV-1, HSV-2, VZV, and PRV are the causative agents of a variety of neurological disorders and diseases (Steiner et al., 2007). The cellular and molecular underpinnings of alphaherpesvirus-inflicted neuronal damage are central to understanding the cause of symptoms and pathogenesis that occur during infection.

Like most large DNA viruses, alphaherpesviruses encode proteins known to perturb mitochondrial function and localization, primarily to block apoptotic response pathways (Pomeranz et al., 2005). For example, the highly conserved pUS3 family of serine/threonine kinases are some of the most potent and best characterized alphaherpesvirus antiapoptotic proteins that protect cells during infection by direct or indirect interactions with Bcl-2 family proteins (Munger et al., 2001; Ogg et al., 2004). Other alphaherpesviral proteins with antiapoptotic functions include: pUL7, pUL54, pUS1, pUS5, pUS6, and ICP34.5 (Pomeranz et al., 2005). Additionally, HSV-1 pUL12.5, which localizes to mitochondria, degrades the mitochondrial genome early during infection (Saffran et al., 2007). Herpesviral proteins also affect mitochondrial location in the infected cell. Murata et al. demonstrated that during HSV-2 infection of epithelial cells, mitochondria cluster around a perinuclear region of the cytoplasm that is enriched with the viral tegument proteins pUL41 and pUL46 (Murata et al., 2000). However, the molecular mechanisms underlying such redistribution of mitochondria during viral infection, as well as the viral and cellular proteins required for this process, have not been characterized.

Mitochondrial distribution within a cell is dependent upon the microtubule cytoskeleton and requires the plus-end directed molecular motor kinesin-1 (KIF5) and the minus-end directed motor dynein for efficient bidirectional transport in axons and dendrites (Hollenbeck and Saxton, 2005). In addition, mitochondrial motion is regulated by the local concentration of calcium ions. Mitochondria stop moving in the presence of elevated [Ca^{2+}] at active synapses (Macaskill et al., 2009; Saotome et al., 2008; Wang and Schwarz, 2009). Cellular proteins, known as Mitochondrial Rho GTPases (Miro 1 and Miro 2), play central roles in this regulatory pathway (Fransson et al., 2003). These proteins localize to the outer mitochondrial membrane and have two calcium-binding EF hand domains that regulate the activity of both kinesin-1 and dynein, as well as the interactions of these motors with mitochondrial protein complexes (Fransson et al., 2006). As a result, Miro proteins serve as calcium sensors that regulate mitochondrial mobility in response to increased synaptic activity and action potential (AP) firing (Li et al., 2004; Macaskill et al., 2009). We have found that after PRV infection of superior cervical ganglia (SCG) neurons in culture, AP firing increases dramatically (McCarthy et al., 2009). Since AP firing results in transient increases in intracellular calcium, we wanted to test the hypothesis that mitochondrial motion would be affected in PRV infected neurons.

In this study, we have performed an analysis of mitochondrial dynamics during alphaherpesvirus infection. We show that mitochondrial motility and morphology are significantly altered during PRV infection of SCG neurons grown in culture. Our results suggest that disruption of mitochondrial motility is a pathogenic effect of infection that is required for efficient viral spread.

RESULTS

Axonal transport of mitochondria is disrupted during PRV and HSV-1 infection

Dissociated rat superior cervical ganglion (SCG) neurons were cultured *in vitro* under tissue culture conditions where only axons, but not dendrites, are produced (Ch'ng et al., 2005; Tomishima and Enquist, 2001). Mitochondria were labeled with the mitochondrial-selective dye MitoTracker Red and visualized by live cell imaging of regions of the tissue culture dish

that contained only axons and not cell bodies. On average, 40.4 ± 2.1% of mitochondria were motile in axons of mock infected neurons (Figure 1A, 1B, and Movie S1). This figure is consistent with previously published studies (Ligon and Steward, 2000). We next sought to assess the effect of PRV infection on mitochondrial motility in axons. For each infection condition, viral inoculum containing 10^6 plaque forming units (PFUs; titered on epithelial cells) was added to ensure a synchronous infection of all neurons in the culture as previously demonstrated (McCarthy et al., 2009). In comparison with mock infected neurons, mitochondrial motility was severely disrupted following infection with PRV Becker (wild type) (Figure 1B and Movie S1). While the percentage of motile mitochondria decreased at the onset of infection (26.3 ± 2.1% at 0–4 hpi), the most dramatic decrease in motility was observed beginning at 12–16 hours post infection (hpi) (4.0 ± 0.7%). To ensure that axonal transport of other cargoes can still occur in these cultures, we simultaneously imaged capsids (labeled with GFP) and mitochondria (labeled with MitoTracker Red). At 12 hpi, we observed robust capsid motility in axons even though mitochondrial motility was disrupted (Movie S1). The percentage of motile mitochondria remained reduced (compared to mock) over the course of PRV infection, even at the latest time point that we measured (72hpi; Figure 1B).

To test whether disruption of mitochondrial motility occurs during infection with another alphaherpesvirus, we infected neurons with the wild type HSV-1 strain KOS. Mitochondrial motility in axons of HSV-1 infected neurons was reduced to 18.6 ± 1.7% by 12–14 hpi and 5.7 ± 1.5% at 16–18 hpi. Thus, mitochondrial motility is also disrupted during HSV-1 infection (Figure 1C and Movie S1).

Since MitoTracker Red stains mitochondria with an active membrane potential, we wanted to ensure that our analysis was not biased towards visualizing only healthy mitochondria with intact membranes. We therefore co-stained mock and infected neurons with both MitoTracker Red and MitoTracker Green, which labels mitochondria regardless of their membrane potential (Ligon and Steward, 2000). In both mock and infected neurons (at 16 hpi), the staining pattern of these two dyes was virtually identical; nearly all of the mitochondria co-labeled with both dyes. This was unchanged even at 24 hpi (Figure S1). Therefore, we conclude that despite causing a severe disruption of mitochondrial motility, PRV infection does not increase mitochondrial membrane permeability or damage compared to mock infected neurons. These results are consistent with evidence that PRV infected neurons are viable at early stages of infection and can support all of the functions that are necessary to complete an infectious cycle. For example, infected cells synthesize viral proteins (Pomeranz et al., 2005) and transport viral cargo (Movie S1; Antinone and Smith, 2006). In addition, infected neurons are able to fire action potentials (McCarthy et al., 2009). We therefore conclude that infected cells grown in our culture conditions are viable and that mitochondrial membrane permeability does not increase during PRV infection.

Disruption of mitochondrial motility is dependent on increased action potential firing during infection

Mitochondrial mobility is reduced in neurons when synaptic activity and action potential (AP) firing are increased (Li et al., 2004; Macaskill et al., 2009). Previously, we have shown that beginning at 8–10 hpi, PRV infected neurons become electrically coupled, a phenomenon which results in the propagation of spontaneous electrical activity with elevated AP firing rates (McCarthy et al., 2009). We therefore tested the hypothesis that this increase in AP firing during PRV infection is required for disruption of mitochondrial motility. AP firing rates do not increase in neurons infected with a PRV strain that does not express glycoprotein B (gB), an essential member of the viral membrane fusion complex (McCarthy et al., 2009). The gB-null strain replicates with equivalent kinetics to wild type PRV (Favoreel et al., 2002), but does not facilitate the formation of fusion pores that are

required for electrical coupling of neurons during infection (Curanovic and Enquist, 2009; McCarthy et al., 2009). We observed that more mitochondria were motile in neurons infected with a gB-null mutant beginning at 12–16 hpi compared to neurons infected with PRV Becker (17.3 ± 1.2% and 4.0 ± 0.7%, respectively) (Figure 1B and Movie S1). Elevated mitochondrial motility in neurons infected with the gB-null strain was observed as late as 24 hpi, but was reduced at later times post infection. Treatment of PRV Becker infected neurons with tetrodotoxin (TTX), a potent inhibitor of AP firing, partially restored mitochondrial motility in infected cells (16.5 ± 2.4% in TTX treated) (Figure 1D). TTX treatment did not alter mitochondrial motility in neurons that were mock infected or infected with a gB-null strain of PRV. Combined, these results suggest that elevated AP firing during infection is required for efficient disruption of mitochondrial motility and that the inhibition of motility is partially reversible.

Mitochondrial morphology is altered during PRV infection

Arrest of mitochondrial transport during infection, and the dependence of this phenomenon on elevated AP firing, is consistent with the findings of previous studies on regulation of mitochondrial dynamics through the Ca^{2+}-sensitive mitochondrial membrane protein Miro (Macaskill et al., 2009; Wang and Schwarz, 2009). In addition to regulating motility, Miro functions as a Ca^{2+}-dependent modulator of mitochondrial morphology by activating mitochondrial fission proteins when intracellular [Ca^{2+}] is increased (Saotome et al., 2008), resulting in a shortening of mitochondrial length. In axons of PRV infected neurons, the mean mitochondrial length was reduced compared to mock infected (0.77 ± 0.02 μm and 1.5 ± 0.03 μm, respectively) (Figure 2A and 2B). Under conditions where AP firing is not elevated or is inhibited during infection, the mean mitochondrial length was increased compared to wild type PRV infection (1.1 ± 0.02 μm for PRV gB-null infected and 1.2 ± 0.02 μm for PRV Becker infected treated with TTX) (Figure 2A and 2B).

Intracellular [Ca^{2+}] increases over the course of PRV infection

To test directly if [Ca^{2+}] changes in neurons over the course of infection, neurons were labeled with the Ca^{2+}-sensitive fluorescent dye Oregon Green 488 BAPTA-1 AM (OGB-1) and imaged at a rate of one frame every 10 minutes from 3–22 hpi (19 hours total). Compared to mock infected neurons, the cell bodies of PRV Becker infected neurons became more fluorescent over this time period, indicating that intracellular [Ca^{2+}] increases over the course of infection (Figure 3A and 3B). Furthermore, beginning at 8–10 hpi, PRV Becker infected neurons exhibited fluorescent flashes representing changes in intracellular [Ca^{2+}] (Figure 3A and Movie S2). This observation coincides with the onset of increased AP firing rates (McCarthy et al., 2009). Moreover, because all of the neurons in the same region of interest flashed synchronously, these Ca^{2+} changes likely result from electrical coupling during infection. No such changes were observed in mock infected neurons. Similarly, intracellular [Ca^{2+}] did not increase in gB-null infected neurons, indicating that the elevation in intracellular [Ca^{2+}] during infection is linked to neuronal membrane fusion and electrical coupling (Figure 3A and 3B). Previously, our lab described an attenuated PRV strain (PRV Bartha) that expresses the genetically encoded Ca^{2+}-sensitive fluorophore G-CaMP2. This study demonstrated that changes in fluorescence were correlated with AP firing during PRV infection of SCG neurons *in vitro* (Granstedt et al., 2009).

To test whether the increase in intracellular [Ca^{2+}] is required for efficient disruption of mitochondrial motility during infection, PRV Becker infected neurons were treated with the Ca^{2+} chelator EGTA (to chelate extracellular Ca^{2+}) or the voltage gated Ca^{2+} channel blocker $CdCl_2$. Under both of these treatments, we noted a small but statistically significant increase in mitochondrial motility compared to untreated (9.3 ± 0.9% for EGTA and 7.6 ± 0.7% for $CdCl_2$). These treatments had a modest effect on decreasing intracellular [Ca^{2+}] in

PRV infected neurons as measured by OGB-1 fluorescence (Figure S2B). These results suggest that influx of Ca^{2+} through voltage gated Ca^{2+} channels during infection is partially responsible for the disruption of mitochondrial motility. However, the increase in AP firing rates observed during infection may trigger Ca^{2+} release into the cytoplasm from other sources, such as the endoplasmic reticulum.

The transport kinetics of the small pool of motile mitochondria is altered during infection

Despite a severe disruption of mitochondrial transport beginning at 12–16 hpi, approximately 5% of mitochondria remained motile during infection. Furthermore, this small fraction was persistently observed even at 20–24 hpi, which was the latest time point when motility was measured (Figure 1B). We therefore determined if this pool of mitochondria that remained motile during infection displayed similar transport kinetics and directionality to motile mitochondria in mock infected neurons. To assess this, we modified our culture system to distinguish whether mitochondria were moving in the anterograde or retrograde direction in axons. Under these culture conditions, we observed that the majority of mitochondria in mock infected cells moved in the anterograde direction (58.0 ± 2.7%), a figure that is consistent with previous studies (Ligon and Steward, 2000). However, in axons of PRV infected neurons at 12–16 hpi, more mitochondria moved in the retrograde direction than in the anterograde direction (Figure 4A). Additionally, during PRV infection, average velocities in both the anterograde and retrograde directions were reduced (Figure 4B). Finally, in infected neurons, both the anterograde and the retrograde run lengths were shorter compared to mock infected (Figure 4C). Overall, these results suggest that in addition to a severe disruption in mitochondrial motility, the transport kinetics of the remaining motile mitochondria are altered during infection.

PRV infection alters the interaction of kinesin-1 heavy chain with mitochondria

Mitochondria utilize microtubule-dependent molecular motor proteins for efficient long distance transport within neurons. Considering the dramatic alteration in mitochondrial transport dynamics during infection, we reasoned that mitochondrial motor protein activity or binding may be altered. We therefore tested if various motor protein subunits known to transport mitochondria remain associated after PRV infection. Since it is difficult to culture a sufficient quantity of primary neurons for biochemical analyses, we took advantage of PC12 cells, a widely used rat pheochromocytoma cell line that produces neurites in the presence of nerve growth factor (NGF) and acquires many of the characteristics of sympathetic neurons (Greene and Tischler, 1976). PC12 cells are susceptible and permissive to PRV infection and have been previously used for studying transport dynamics of viral particles in axons (Lyman et al., 2008). We therefore enriched mitochondria from mock and PRV infected PC12 cells and probed for the presence or absence of various motor protein subunits using western blot analysis.

Notably, kinesin-1 heavy chain (HC) was depleted from mitochondria that were enriched from PRV infected PC12 cells (Figure 5A). Kinesin-1 HC is the primary motor responsible for plus-end microtubule-dependent transport of mitochondria (Hollenbeck and Saxton, 2005). In contrast, we did not detect a change in the levels of the kinesin-3 family member KIF1Bα, which has been previously shown to transport mitochondria along microtubules *in vitro* (Nangaku et al., 1994). Furthermore, retrograde motion of mitochondria along microtubules in axons is dependent on cytoplasmic dynein (Hollenbeck and Saxton, 2005). We did not detect a change in the levels of the dynein intermediate chain IC74 in mitochondria isolated from mock and PRV infected cells (Figure 5A). This suggests a potential explanation for the reduction in plus-end directed (anterograde) mitochondrial motility in axons of PRV infected neurons (Figure 4).

To assess when depletion of kinesin-1 HC occurs during PRV infection, we enriched mitochondria from samples collected at different times post infection. Since Miro1 is anchored in the mitochondrial membrane and is required for recruitment of kinesin-1 HC, we normalized the levels of kinesin-1 HC to those of Miro1 within the enriched mitochondrial fraction at each time point. We found that disruption of kinesin-1 HC binding to mitochondria was a gradual process, with the greatest depletion occurring late during infection (after 12 hpi; Figure 5B). This timing is consistent with the most severe disruption of mitochondrial motility late during PRV infection (between 12–16 hpi, Figure 1B). Co-immunoprecipitation experiments confirmed that the association of kinesin-1 HC, but not dynein IC74, with Miro1 is reduced during PRV infection (Figure 5C). Overall, these experiments suggest that PRV infection changes mitochondrial transport kinetics by disrupting kinesin-1 HC recruitment to mitochondria through Miro1.

Disruption of mitochondrial motility during infection is dependent on the Ca^{2+} -sensitive EF hand domains of Miro

Previous studies have shown that Miro has two Ca^{2+}-sensitive EF-hand domains that are required for regulating motor protein recruitment and activity. When Ca^{2+} is elevated in neurons due to increased firing or pharmacological treatment, proper function of these motifs is required for arrest of mitochondrial motility (Macaskill et al., 2009; Saotome et al., 2008; Wang and Schwarz, 2009). Since PRV infection results in elevated intracellular [Ca^{2+}] and disruption of kinesin-1 HC binding to mitochondria through Miro, we hypothesized that Miro's Ca^{2+}-sensitive function is required for efficient disruption of mitochondrial motility during infection. To test this, we compared mitochondrial dynamics in PRV infected neurons that express GFP-tagged wild type (GFP-Miro1) and mutated Miro proteins in which the EF hands have been disrupted by changing essential glutamates to lysines (GFP-Miro1ΔEF) (Fransson et al., 2006). Similar constructs have previously been used to study Miro-dependent regulation of mitochondrial dynamics (Fransson et al., 2006). Since transfection of SCG neurons is inefficient, we inserted expression cassettes for these constructs into the PRV genome in a region that is nonessential for growth and spread *in vitro* (Banfield and Bird, 2009) (Figure 6A). This strategy ensured that each infected neuron would express one of these two proteins. By fluorescence microscopy, we found that these constructs properly localized to mitochondria in axons of infected neurons that were co-labeled with MitoTracker Red (Figure S3A). Western blot analysis showed that cells infected with these viruses express similar levels of GFP-tagged proteins of expected size (Figure S3B).

Compared to PRV Becker or PRV infected neurons expressing wild type GFP-Miro1 (PRV 197, here referred to as PRV Miro1), mitochondrial motility was increased in neurons expressing GFP-Miro1ΔEF (PRV 198, here referred to as PRV Miro1ΔEF) at 12–16 hpi (% motile mitochondria: 4.0 ± 0.7% for PRV Becker, 3.8 ± 0.4% for PRV Miro1, and 13.9 ± 0.5% for PRV Miro1ΔEF) (Figures 6B, 6D, and Movie S3). Furthermore, mitochondrial length was increased in neurons infected with PRV Miro1ΔEF compared to PRV Becker or PRV Miro1 infected (0.88 ± 0.02 μm for PRV Becker, 1.05 ± 0.02 μm for PRV Miro1, and 1.4 ± 0.02 μm for PRV Miro1ΔEF; Figure 6C). We conclude that effective disruption of mitochondrial motility and morphology during infection is dependent on the Ca^{2+}-sensitive motifs of Miro.

Efficient growth and spread of PRV is dependent upon disruption of mitochondrial motility through the EF hand domains of Miro

Since disruption of mitochondrial dynamics is required for efficient infection by other pathogens (Stavru et al., 2011), we next asked whether this phenomenon was also important

for efficient alphaherpesvirus infection. We thus compared the growth and spread properties of the PRV strains expressing wild type and mutant EF hand Miro proteins.

Viruses that are defective in growth or spread often exhibit a small plaque size phenotype (Tirabassi and Enquist, 1999). Therefore, we analyzed plaques formed on epithelial cells (PK15 cells) by PRV 151 (expresses diffusible GFP; hereon referred to as PRV GFP; Figure 7A), PRV Miro1, and PRV Miro1ΔEF. The diameters of the plaques formed at 48 hpi by PRV Miro1ΔEF were significantly smaller than those formed by PRV GFP and PRV Miro1 (mean plaque size: 614.0 ± 5.9 μm for PRV GFP, 547.4 ± 5.5 μm for PRV Miro1, and 276.8 ± 2.9 μm for PRV Miro1ΔEF; Figures 7A and 7B). Three independently isolated clones of PRV Miro1 and PRV Miro1ΔEF displayed similar phenotypes (Figure S3C). Next, to assess the growth kinetics of these strains, we performed single step growth curves in PK15 cells. Compared to PRV GFP and PRV Miro1, growth of PRV Miro1ΔEF was kinetically delayed during the earlier stages of infection but was equivalent by 24 hpi. The growth curves for both the extracellular and cell associated fractions exhibited similar patterns (Figure 7C and 7D). Combined, these results suggest that Miro's Ca^{2+}-sensing function is required for efficient spread and growth of PRV in non-neuronal cells.

To test whether disruption of mitochondrial motility through Miro function is important for spread in neurons, we took advantage of a compartmentalized neuronal culture system (Ch'ng and Enquist, 2005). In this system, dissociated SCG neurons are seeded in the soma (S) compartment and allowed to mature for two weeks. During this period, axons grow through grooves across the methocellulose (M) compartment and extend into the neurite (N) chamber. Prior to infection, indicator PK15 cells are plated on top of the neurites in the N compartment to amplify virus and facilitate detection of anterograde spread. When neuron cell bodies in the S compartment are infected, virus particles spread into the N compartment exclusively through the axons that extend and contact PK15 cells. Thus, this system can be used to assess the efficiency of anterograde sorting and spread of different virus strains in neurons *in vitro*.

Using this system, we compared the anterograde spread capabilities of PRV GFP, PRV Miro1, and PRV Miro1ΔEF (Figure 7E). For all of these strains, there was no significant difference in the viral titers in the S compartment at 24 hpi, consistent with the growth curves shown in Figure 7C and 7D. However, spread to the N compartment was reduced more than 10-fold in chambers infected with PRV Miro1ΔEF compared to those infected with PRV GFP or PRV Miro1. While our chamber assay is dependent upon the presence of a detector layer of PK15 cells in the N compartment, PRV Miro1ΔEF reached equivalent titers by 24 hpi (Figures 7C and 7D). This is the same time point at which we harvested the S and N compartments of our chambers (Figure 7E). This suggests that the ability of Miro to sense changes in intracellular [Ca^{2+}] through its EF hand domains and modulate mitochondrial dynamics is required for efficient neuronal spread of PRV *in vitro*.

Overall, we conclude that efficient disruption of mitochondrial motility during infection is dependent on Miro's Ca^{2+}-sensitive function. Additionally, from the three assays presented in Figure 7, efficient disruption of mitochondrial motility though Miro function is required for growth and spread of PRV.

DISCUSSION

Mitochondria are important for many essential cellular processes such as meeting metabolic demands, maintaining Ca^{2+} homeostasis, and regulating apoptosis. Thus, it is not surprising that defects in mitochondrial function are implicated in many well-known neurodegenerative disorders, including Alzheimer's disease (AD), Parkinson's disease (PD), amyotrophic lateral

sclerosis (ALS), and Huntington's disease (HD) (Sheng and Cai, 2012). Moreover, an increasing number of microbial pathogens, including viruses and bacteria, alter mitochondrial dynamics during infection (Ohta and Nishiyama, 2011). Here we show that neuroinvasive alphaherpesviruses cause a dramatic alteration of mitochondrial motility and morphology in neurons *in vitro*. This represents a pathogenic effect of alphaherpesvirus infection in neurons. Based on our findings, we suggest that disruption of mitochondrial dynamics is an epiphenomenon resulting from a series of convergent events that occur during infection (Figure 7F).

Previously, McCarthy et al. showed that expression of viral membrane fusion proteins, such as gB, during infection leads to the formation of fusion pores at sites where neuronal membranes are in close contact. These pores allow for the free flow of ions and electrical signals between cells, thus allowing rare and spontaneous APs that occur in one neuron to propagate throughout the entire network. Therefore, PRV infection results in elevated and synchronous AP firing activity beginning at 8–10 hpi by electrical (not synaptically mediated) coupling of neurons (McCarthy et al., 2009).

In this study, we show that the alteration in neuronal electrical activity is required for efficient disruption of mitochondrial dynamics during infection (Figures 1 and 2). Importantly, over the course of PRV infection, we observed a dramatic increase in intracellular [Ca^{2+}] compared to mock infected cells (Figures 3A and 3B). Consequently, mitochondrial motility and morphology are altered due to the function of Miro (Figure 6B and 6C), a protein that regulates mitochondrial dynamics in response to changes in intracellular Ca^{2+}. According to our model, this leads to alteration of mitochondrial motor protein activity (Figure 4), including a disruption in kinesin-1 HC recruitment (Figure 5), and a significant reduction in motility after 12 hpi (Figure 7F).

While elevated AP firing is required for efficient disruption of mitochondrial motility during infection, additional mechanisms likely contribute to this phenomenon. As evidence of this, we still observed a decrease in motility in neurons infected with a PRV strain that is gB-null, a condition during which AP firing rates and intracellular [Ca^{2+}] do not increase during infection. Additionally, we observed a reduction in motility as soon as 0–4 hpi, prior to the onset of elevated AP firing activity (McCarthy et al., 2009). Thus, we conclude that additional viral or cellular pathways may play a role in disrupting motility. While Miro-dependent Ca^{2+}-sensitivity is perhaps the best-characterized regulator of mitochondrial dynamics, other levels of regulation are known to exist. These include proteins such as syntaphilin (Kang et al., 2008) and syntabulin (Cai et al., 2005), or other proteins such as O-GlcNAc transferase (OGT), that may regulate mitochondrial dynamics in response to metabolic changes (Glater et al., 2006). The latter option is appealing since herpesvirus infections, including HSV-1, are known to dramatically alter the metabolic profiles of a variety of cell types to support viral growth (Vastag et al., 2011). Another possibility is that viral proteins function to directly or indirectly disrupt mitochondrial mobility. Candidates include viral proteins that localize to mitochondria, such as pUL7 (Tanaka et al., 2008) and pUL12.5 (Ishihara et al., 2009). These mechanisms may contribute to disruption of motility either alone or in concert.

This disruption of mitochondrial motility is required for efficient growth and spread of PRV. Furthermore, the recruitment of kinesin-1 HC to mitochondria is disrupted through Miro. This raises the possibility that kinesin-1 HC is hijacked and repurposed for movement of viral particles or protein complexes during assembly and/or egress (Figure 7F). This model is speculative, but consistent with previous findings showing that PRV and HSV-1 utilize kinesin-1 for transport (Dodding and Way, 2011). Our findings are also consistent with

previous work indicating that mitochondria accumulate at a perinuclear region of the cytoplasm during HSV-2 infection of epithelial cells (Murata et al., 2000).

Two published models have been proposed to explain how mitochondrial motor protein activity is regulated by the Ca^{2+}-binding EF hands of Miro in response to changes in Ca^{2+} flux. MacAskill et al. showed that Ca^{2+} binding to Miro detaches kinesin-1 HC from mitochondria (Macaskill et al., 2009). In contrast, Wang and Schwarz demonstrated that Ca^{2+}-binding permits Miro to interact directly with the motor domain of kinesin-1 HC, thus preventing its engagement with microtubules (Wang and Schwarz, 2009). Since the percentage of mobile mitochondria during infection is reduced prior to the disruption of kinesin-1 HC binding (Figure 1B and Figure 5), we propose that PRV may disrupt motility through a graduated process involving a combination of these two mechanisms. Prior to 12 hpi, motility is reduced but kinesin-1 HC remains associated with mitochondria, potentially due to “on” and “off” binding of its motor domain to Miro. However, after the onset of elevated AP firing and extended exposure to increased intracellular [Ca^{2+}], Miro proteins release kinesin-1 HC from mitochondria, thus accounting for the sharper decrease in motility observed beginning at 12–16 hpi. Interestingly, Wang et al. recently reported that the Serine/Threonine kinase PINK1 and the ubiquitin ligase Parkin arrest mitochondrial movement by targeting Miro for degradation in response to mitochondrial damage. As a consequence, kinesin-1 HC becomes detached from the surface of mitochondria (Wang et al., 2011). While we did not find evidence that PRV infection resulted in loss of mitochondrial membrane integrity (Figure S1) or Miro degradation (Figure 5B), it is possible that the molecular signs of mitochondrial damage become apparent at later times post infection.

Retrograde motility of mitochondria, which is dependent on dynein motors, was also altered during PRV infection (Figure 4). However, unlike kinesin-1 HC, we did not observe a disruption in dynein IC74 binding during infection (Figure 5A and 5C). Very little is currently known about the molecular details of dynein recruitment and activation on the surface of mitochondria, including which subunits are required. Since dynein is a large multi-subunit complex, one possibility is that dynein heavy chain recruitment is disrupted during infection, but not the intermediate chain IC74 (Hollenbeck and Saxton, 2005). Another possibility is that dynein function on the surface of mitochondria is dependent on the presence of kinesin-1 HC. For several organelles that undergo bidirectional transport, motility in either direction is dependent on simultaneous recruitment of opposite polarity motors (Welte, 2004).

Mutation of Miro’s EF hand domains may have additional implications for PRV growth and spread. In uninfected neurons that are subject to excitotoxic stress, where intracellular [Ca^{2+}] is increased due to elevated neuronal firing activity, the EF hands of Miro function to properly regulate mitochondrial dynamics in order to protect neurons from apoptotic death (Wang and Schwarz, 2009). Our finding that PRV induces a dramatic increase in intracellular [Ca^{2+}] in neurons is significant. It is remarkable that neurons cultured *in vitro* are able to survive for several days post infection (McCarthy et al., 2009) and do not die of excitotoxic Ca^{2+} overload (Pivovarova and Andrews, 2010). This prolonged survival is likely mediated by the functions of viral antiapoptotic proteins, which may have evolved to maintain cell viability in anticipation of excitotoxic and other types of stress that are induced during infection *in vivo*.

If elevated Ca^{2+} flux is cytopathic, why is it induced by PRV infection and is it necessary for efficient progression of the infectious cycle? Since Ca^{2+} signaling is a key regulator of many fundamental cellular processes and facilitates various aspects of infection for many viruses (Chami et al., 2006), the answer to this question is not necessarily straightforward. One hypothesis for its role in PRV infection is that elevated [Ca^{2+}] may facilitate viral

spread of infection at synapses by triggering Ca^{2+}-dependent membrane fusion, similar to the mechanism underlying synaptic vesicle exocytosis. The source of the Ca^{2+} influx remains unknown and its identification may contribute to our understanding of its role during infection. Since intracellular [Ca^{2+}] did not increase in neurons infected with a gB-null PRV strain, Ca^{2+} influx during wild type PRV infection likely results from the effects of elevated AP firing leading to activation of cell-surface voltage gated Ca^{2+} channels. However, Ca^{2+} may also be released into the cytoplasm from other sources. For example, HSV-1 and the betaherpesvirus human cytomegalovirus (HCMV) have been shown to induce Ca^{2+} release from the endoplasmic reticulum (Cheshenko et al., 2003; Sharon-Friling et al., 2006).

Future work will focus on determining whether changes in intracellular [Ca^{2+}] and alteration of mitochondrial dynamics also occur as a result of alphaherpesvirus infection *in vivo*. Multiple clinical and molecular studies of neuronal activity during alphaherpesvirus infection in natural and non-natural hosts suggest that this is likely. Several key symptoms that emerge following human alphaherpesvirus infections may be attributed to alterations in sensory or motor neuron activity (Steiner et al., 2007). Additionally, *in vivo* electrical recordings of PRV infected rat SCG ganglia exhibited increased neuronal firing activity compared to uninfected ganglia (Dempsher et al., 1955; Liao et al., 1991). In agreement with these findings, *in vivo* imaging of submandibular ganglion (SMG) neurons infected PRV Bartha expressing G-CaMP2 exhibited frequent and prolonged Ca^{2+} transients by 72 hpi (Granstedt et al., 2009). Unpublished data from our lab shows that optical recordings of SMG neurons infected with a virulent PRV strain that expresses G-CaMP3 displayed frequent and synchronous Ca^{2+} transients (A.E. Granstedt and L.W. Enquist, personal communication), similar to those that we observed in this study. Thus, although neuronal architecture in host tissues is organized quite differently from that of pure dissociated cultures *in vitro*, these studies support the hypothesis that alteration of neuronal activity during infection is due to PRV-dependent fusion of membranes between synaptically connected neurons and/or surrounding glial cells. Further work is necessary to assess the putative effects of altered neuronal activity and increased Ca^{2+} flux on mitochondrial dynamics *in vivo* and the relevance of this epiphenomenon to alphaherpesvirus pathogenesis.

EXPERIMENTAL PROCEDURES

Viruses, cells, and neuronal cultures

Viral stocks were propagated in cells grown with Dulbecco's Modified Eagle Medium (DMEM) supplemented with 2% fetal bovine serum and 1% penicillin/streptomycin (all from HyClone, Logan, UT). Embryonic rat superior cervical ganglia (SCG) neurons were isolated as described previously (Ch'ng et al., 2005). For infection of SCG neurons, cells were incubated with 10^6 plaque forming units (PFUs; titered on PK15 cells) of the indicated viral strains. The calculated multiplicity of infection (MOI) is around 200 PFUs per cell body plated. These infection conditions have been previously demonstrated to allow for a synchronous infection of all of the neuron cell bodies in the culture dish (Ch'ng et al., 2005; McCarthy et al., 2009). Additional details are provided in the Supplemental Experimental Procedures.

Reagents

Mitotracker Red CMX Ros (10 nM), Mitotracker Green (10 nM), and Oregon Green 488 BAPTA-1 AM (OGB-1; 5 μM) were diluted in sterile DMSO and used according to the manufacturer's instructions (Invitrogen, Carlsbad, CA). Tetrodotoxin (TTX), EGTA, and

$CdCl_2$ were purchased from Sigma-Aldrich (Saint Louis, MO), diluted in tissue culture grade water, and sterile filtered.

Microscopy and image analysis

Imaging experiments were performed on a Nikon Ti-Eclipse inverted epifluorescence microscope (Nikon Instruments, Tokyo, Japan). For analysis of mitochondrial motility, movies of MitoTracker Red stained were acquired at a rate of 1.2 frames per second (for 3 min) in 2,500 μm^2 regions of interest (ROIs) containing at least 100 mitochondria. A total of at least six movies were acquired for each experimental condition from at least two biological replicates. Additional details are provided in the Supplemental Experimental Procedures.

Statistical analysis

One-way ANOVA with Tukey's post-test or the Mann-Whitney *U* test were performed using GraphPad Prism 5.0d for Max OS X (GraphPad Software, San Diego, CA, www.graphpad.com). Numbers included in the bar diagrams, text, and figure legends throughout the manuscript indicate the mean ± SEM. Throughout the manuscript, ns is not significant, * is $p < 0.05$, ** is $p < 0.01$, and *** is $p < 0.001$.

Mitochondrial enrichment and co-immunoprecipitation

NGF differentiated PC12 cells were used for mitochondrial enrichment and co-immunoprecipitation experiments, which were performed as previously described but with modifications (Cristea and Chait, 2011a, b; Wang and Schwarz, 2009). Additional details are provided in the Supplemental Experimental Procedures.

Article Highlights

- Alphaherpesvirus infection of neurons dramatically reduces mitochondrial motion.
- Intracellular $[Ca^{2+}]$ increases due to the action of viral membrane fusion proteins.
- Efficient viral growth and spread require disrupted mitochondrial dynamics.
- Mitochondrial motility disruption is a pathogenic effect of alphaherpesvirus infection.

Supplementary Material

Refer to Web version on PubMed Central for supplementary material.

Acknowledgments

We would like to thank J.M. Scholey, P. Aspenström, and S.T. Brady for generously providing reagents for this study. We would also like to thank M.P. Taylor for assistance with culturing neurons and the trichamber experiments, as well as other members of the Enquist lab for critical reading of this manuscript. This work was supported by National Institutes of Health grants (R37 NS33506, R01 NS060699, and P40 RR18604) to L.W.E. and a National Science Foundation Graduate Research Fellowship (DGE-0646086) to T.K.

REFERENCES

Antinone SE, Smith G. Two modes of herpesvirus trafficking in neurons: membrane acquisition directs motion. J Virol. 2006; 80:11235–11240. [PubMed: 16971439]

Banfield BW, Bird GA. Construction and analysis of alphaherpesviruses expressing green fluorescent protein. Methods Mol Biol. 2009; 515:227–238. [PubMed: 19378130]

Cai Q, Gerwin C, Sheng Z-H. Syntabulin-mediated anterograde transport of mitochondria along neuronal processes. J Cell Biol. 2005; 170:959–969. [PubMed: 16157705]

Ch'ng TH, Enquist LW. Efficient axonal localization of alphaherpesvirus structural proteins in cultured sympathetic neurons requires viral glycoprotein E. J Virol. 2005; 79:8835–8846. [PubMed: 15994777]

Ch'ng TH, Flood EA, Enquist LW. Culturing primary and transformed neuronal cells for studying pseudorabies virus infection. Methods Mol Biol. 2005; 292:299–316. [PubMed: 15507717]

Chami M, Oulès B, Paterlini-Bréchot P. Cytobiological consequences of calcium-signaling alterations induced by human viral proteins. Biochim Biophys Acta. 2006; 1763:1344–1362. [PubMed: 17059849]

Chang DTW, Honick AS, Reynolds IJ. Mitochondrial trafficking to synapses in cultured primary cortical neurons. J Neurosci. 2006; 26:7035–7045. [PubMed: 16807333]

Cheshenko N, Del Rosario B, Woda C, Marcellino D, Satlin LM, Herold BC. Herpes simplex virus triggers activation of calcium-signaling pathways. J Cell Biol. 2003; 163:283–293. [PubMed: 14568989]

Cristea I, Chait B. Affinity Purification of Protein Complexes. Cold Spring Harbor Protocols 2011, pdb.prot5611. 2011a

Cristea I, Chait B. Conjugation of Magnetic Beads for Immunopurification of Protein Complexes. Cold Spring Harbor Protocols 2011, pdb.prot5610. 2011b

Curanovic D, Enquist LW. Virion-Incorporated Glycoprotein B Mediates Transneuronal Spread of Pseudorabies Virus. J Virol. 2009

Dempsher J, Larrabee MG, Bang FB, Bodian D. Physiological changes in sympathetic ganglia infected with pseudorabies virus. Am J Physiol. 1955; 182:203–216. [PubMed: 13248967]

Dodding MP, Way M. Coupling viruses to dynein and kinesin-1. EMBO J. 2011; 30:3527–3539. [PubMed: 21878994]

Favoreel HW, Van Minnebruggen G, Nauwynck HJ, Enquist LW, Pensaert MB. A tyrosine-based motif in the cytoplasmic tail of pseudorabies virus glycoprotein B is important for both antibody-induced internalization of viral glycoproteins and efficient cell-to-cell spread. J Virol. 2002; 76:6845–6851. [PubMed: 12050399]

Fransson A, Ruusala A, Aspenström P. Atypical Rho GTPases have roles in mitochondrial homeostasis and apoptosis. J Biol Chem. 2003; 278:6495–6502. [PubMed: 12482879]

Fransson S, Ruusala A, Aspenström P. The atypical Rho GTPases Miro-1 and Miro-2 have essential roles in mitochondrial trafficking. Biochem Biophys Res Commun. 2006; 344:500–510. [PubMed: 16630562]

Glater EE, Megeath LJ, Stowers RS, Schwarz TL. Axonal transport of mitochondria requires milton to recruit kinesin heavy chain and is light chain independent. J Cell Biol. 2006; 173:545–557. [PubMed: 16717129]

Granstedt AE, Szpara ML, Kuhn B, Wang SS-H, Enquist LW. Fluorescence-based monitoring of in vivo neural activity using a circuit-tracing pseudorabies virus. PLoS ONE. 2009; 4:e6923. [PubMed: 19742327]

Greene LA, Tischler AS. Establishment of a noradrenergic clonal line of rat adrenal pheochromocytoma cells which respond to nerve growth factor. Proc Natl Acad Sci USA. 1976; 73:2424–2428. [PubMed: 1065897]

Hollenbeck PJ, Saxton WM. The axonal transport of mitochondria. Journal of Cell Science. 2005; 118:5411–5419. [PubMed: 16306220]

Ishihara N, Nomura M, Jofuku A, Kato H, Suzuki SO, Masuda K, Otera H, Nakanishi Y, Nonaka I, Goto Y-i, et al. Mitochondrial fission factor Drp1 is essential for embryonic development and synapse formation in mice. Nat Cell Biol. 2009; 11:958–966. [PubMed: 19578372]

Kang J-S, Tian J-H, Pan P-Y, Zald P, Li C, Deng C, Sheng Z-H. Docking of axonal mitochondria by syntaphilin controls their mobility and affects short-term facilitation. Cell. 2008; 132:137–148. [PubMed: 18191227]

Li Z, Okamoto K-I, Hayashi Y, Sheng M. The importance of dendritic mitochondria in the morphogenesis and plasticity of spines and synapses. Cell. 2004; 119:873–887. [PubMed: 15607982]

Liao GS, Maillard M, Kiraly M. Ion channels involved in the presynaptic hyperexcitability induced by herpes virus suis in rat superior cervical ganglion. Neuroscience. 1991; 41:797–807. [PubMed: 1714555]

Ligon LA, Steward O. Movement of mitochondria in the axons and dendrites of cultured hippocampal neurons. J Comp Neurol. 2000; 427:340–350. [PubMed: 11054697]

Lyman MG, Curanović D, Enquist LW. Targeting of pseudorabies virus structural proteins to axons requires association of the viral Us9 protein with lipid rafts. PLoS Pathogens. 2008; 4:e1000065. [PubMed: 18483549]

Macaskill AF, Rinholm JE, Twelvetrees AE, Arancibia-Carcamo IL, Muir J, Fransson A, Aspenstrom P, Attwell D, Kittler JT. Miro1 is a calcium sensor for glutamate receptor-dependent localization of mitochondria at synapses. Neuron. 2009; 61:541–555. [PubMed: 19249275]

McCarthy KM, Tank DW, Enquist LW. Pseudorabies virus infection alters neuronal activity and connectivity in vitro. PLoS Pathogens. 2009; 5:e1000640. [PubMed: 19876391]

Munger J, Chee AV, Roizman B. The U(S)3 protein kinase blocks apoptosis induced by the d120 mutant of herpes simplex virus 1 at a premitochondrial stage. J Virol. 2001; 75:5491–5497. [PubMed: 11356956]

Murata T, Goshima F, Daikoku T, Inagaki-Ohara K, Takakuwa H, Kato K, Nishiyama Y. Mitochondrial distribution and function in herpes simplex virus-infected cells. J Gen Virol. 2000; 81:401–406. [PubMed: 10644838]

Nangaku M, Sato-Yoshitake R, Okada Y, Noda Y, Takemura R, Yamazaki H, Hirokawa N. KIF1B, a novel microtubule plus end-directed monomeric motor protein for transport of mitochondria. Cell. 1994; 79:1209–1220. [PubMed: 7528108]

Ogg PD, McDonell PJ, Ryckman BJ, Knudson CM, Roller RJ. The HSV-1 Us3 protein kinase is sufficient to block apoptosis induced by overexpression of a variety of Bcl-2 family members. Virology. 2004; 319:212–224. [PubMed: 14980482]

Ohta A, Nishiyama Y. Mitochondria and viruses. Mitochondrion. 2011; 11:1–12. [PubMed: 20813204]

Pellett, PE.; Roizman, B. The Family: Herpesviridae A Brief Introduction. 5th edn. Vol. Vol 2. Philadelphia, PA: Lippincott, Williams, and Wilkins; 2007.

Pivovarova NB, Andrews SB. Calcium-dependent mitochondrial function and dysfunction in neurons. FEBS J. 2010; 277:3622–3636. [PubMed: 20659161]

Pomeranz LE, Reynolds AE, Hengartner CJ. Molecular biology of pseudorabies virus: impact on neurovirology and veterinary medicine. Microbiology and Molecular Biology Reviews. 2005; 69:462–500. [PubMed: 16148307]

Saffran HA, Pare JM, Corcoran JA, Weller SK, Smiley JR. Herpes simplex virus eliminates host mitochondrial DNA. EMBO Rep. 2007; 8:188–193. [PubMed: 17186027]

Saotome M, Safiulina D, Szabadkai G, Das S, Fransson A, Aspenstrom P, Rizzuto R, Hajnóczky G. Bidirectional Ca2+-dependent control of mitochondrial dynamics by the Miro GTPase. Proc Natl Acad Sci USA. 2008; 105:20728–20733. [PubMed: 19098100]

Sharon-Friling R, Goodhouse J, Colberg-Poley AM, Shenk T. Human cytomegalovirus pUL37x1 induces the release of endoplasmic reticulum calcium stores. Proc Natl Acad Sci USA. 2006; 103:19117–19122. [PubMed: 17135350]

Sheng Z-H, Cai Q. Mitochondrial transport in neurons: impact on synaptic homeostasis and neurodegeneration. Nature Reviews Neuroscience. 2012

Stavru F, Bouillaud F, Sartori A, Ricquier D, Cossart P. Listeria monocytogenes transiently alters mitochondrial dynamics during infection. Proceedings of the National Academy of Sciences. 2011

Steiner I, Kennedy PGE, Pachner AR. The neurotropic herpes viruses: herpes simplex and varicella-zoster. Lancet neurology. 2007; 6:1015–1028. [PubMed: 17945155]

Tanaka M, Sata T, Kawaguchi Y. The product of the Herpes simplex virus 1 UL7 gene interacts with a mitochondrial protein, adenine nucleotide translocator 2. Virol J. 2008; 5:125. [PubMed: 18940012]

Tirabassi RS, Enquist LW. Mutation of the YXXL endocytosis motif in the cytoplasmic tail of pseudorabies virus gE. J Virol. 1999; 73:2717–2728. [PubMed: 10074118]

Tomishima MJ, Enquist LW. A conserved alpha-herpesvirus protein necessary for axonal localization of viral membrane proteins. J Cell Biol. 2001; 154:741–752. [PubMed: 11502759]

Vastag L, Koyuncu E, Grady SL, Shenk TE, Rabinowitz JD. Divergent effects of human cytomegalovirus and herpes simplex virus-1 on cellular metabolism. PLoS Pathogens. 2011; 7:e1002124. [PubMed: 21779165]

Wang X, Schwarz TL. The mechanism of Ca2+ -dependent regulation of kinesin-mediated mitochondrial motility. Cell. 2009; 136:163–174. [PubMed: 19135897]

Wang X, Winter D, Ashrafi G, Schlehe J, Wong YL, Selkoe D, Rice S, Steen J, Lavoie MJ, Schwarz TL. PINK1 and Parkin Target Miro for Phosphorylation and Degradation to Arrest Mitochondrial Motility. Cell. 2011; 147:893–906. [PubMed: 22078885]

Welte MA. Bidirectional transport along microtubules. Curr Biol. 2004; 14:R525–R537. [PubMed: 15242636]

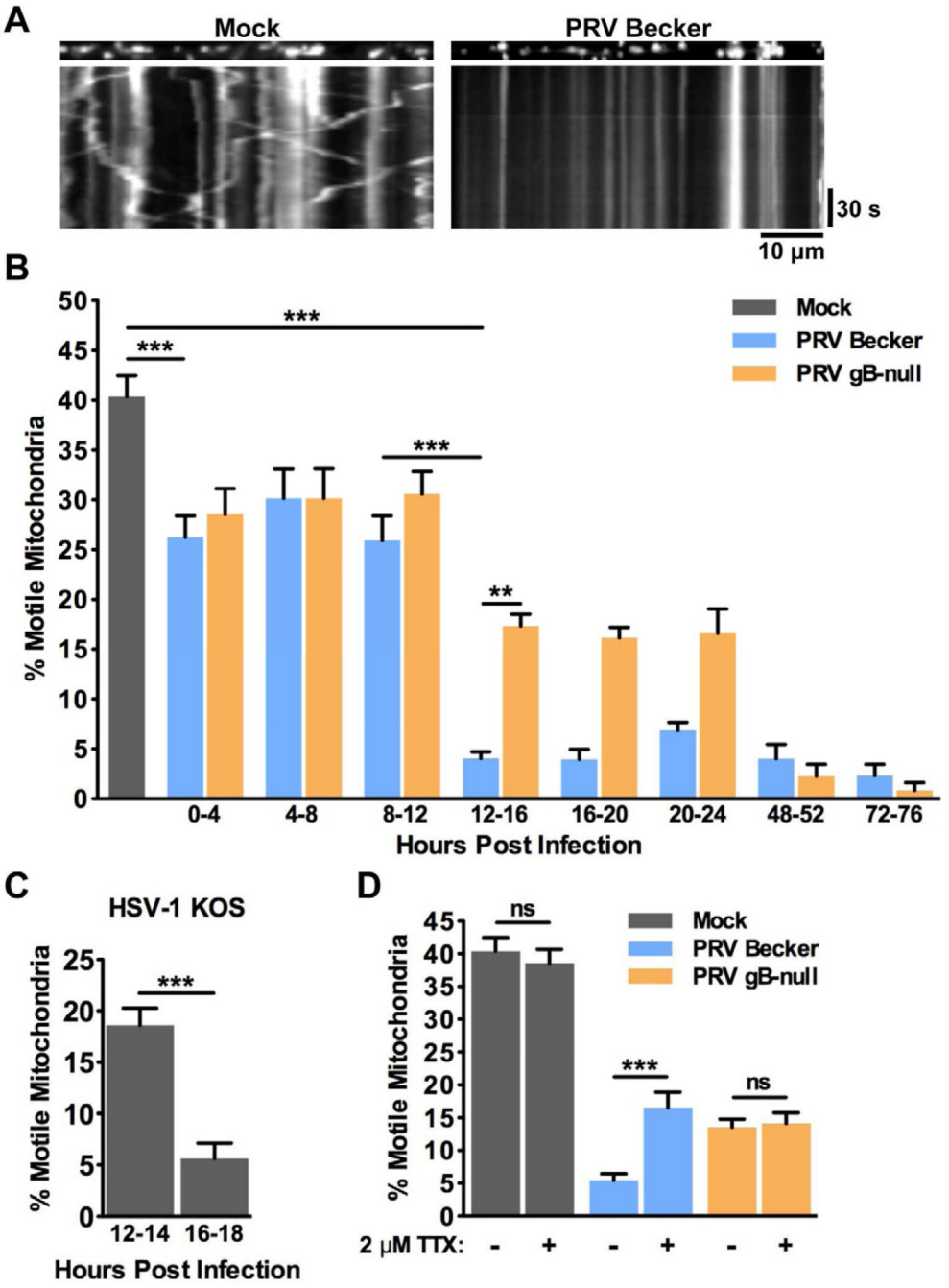

Figure 1. Mitochondrial motility is disrupted during alphaherpesvirus infection in neurons

(A) Kymographs of MitoTracker Red labeled mitochondria in axons from mock (left panels) and PRV Becker (wild type virulent strain; right panels) infected SCG neurons at 16 hpi. Vertical lines represent stationary mitochondria and diagonal lines represent motile mitochondria. (B) The percentage of motile mitochondria in axons from mock, PRV Becker, PRV gB-null infected neurons. The indicated time points are non-overlapping. Throughout the paper, for each condition in each time point the percentage of motile mitochondria was calculated from at least six movies (three minutes each) from at least two biological replicates. Each movie contained at least 100 mitochondria. See Experimental Procedures for more details. (C) The percentage of motile mitochondria in axons of HSV-1 KOS

infected neurons. (D) The percentage of motile mitochondria in axons of mock or PRV infected neurons at 16–18 in the presence or absence of 2 μM tetrodotoxin (TTX). TTX was applied at 15 hpi, 1 hour prior to imaging. See also Figure S1 and Movie S1. Error bars represent mean ± SEM. Throughout the paper, ns is not significant, * is $p < 0.05$, ** is $p < 0.01$, and *** is $p < 0.001$.

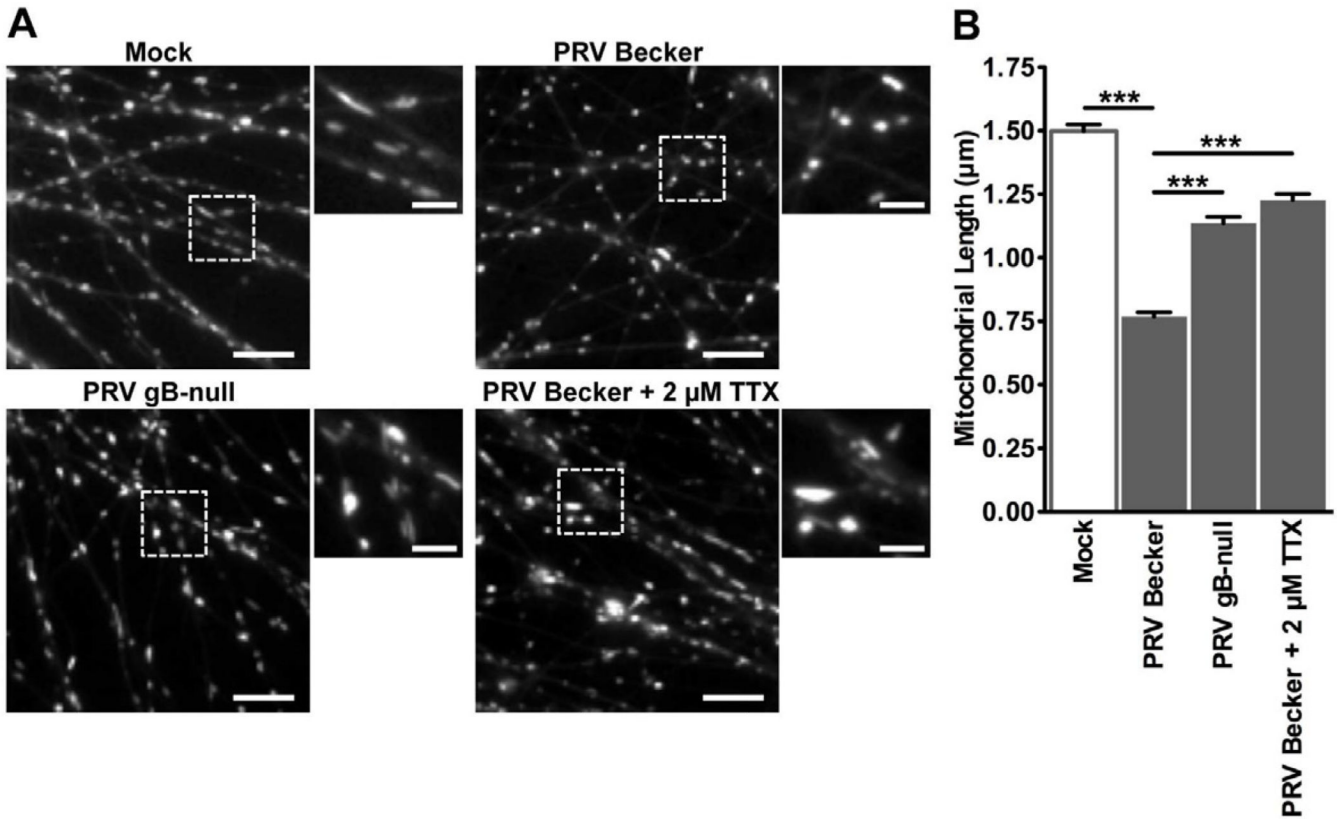

Figure 2. Mitochondrial morphology is altered during PRV infection

(A) Representative ROIs containing MitoTracker Red labeled mitochondria in axons from mock or PRV infected neurons (scale bars = 10 μm). Magnified portions are shown to the right of each image (scale bars = 3 μm). (B) Quantification of mitochondrial length at 16 hpi (n≥700 mitochondria per condition from at least six images that were acquired for each experimental condition from at least two biological replicates). Error bars represent mean ± SEM. See also Movie S1.

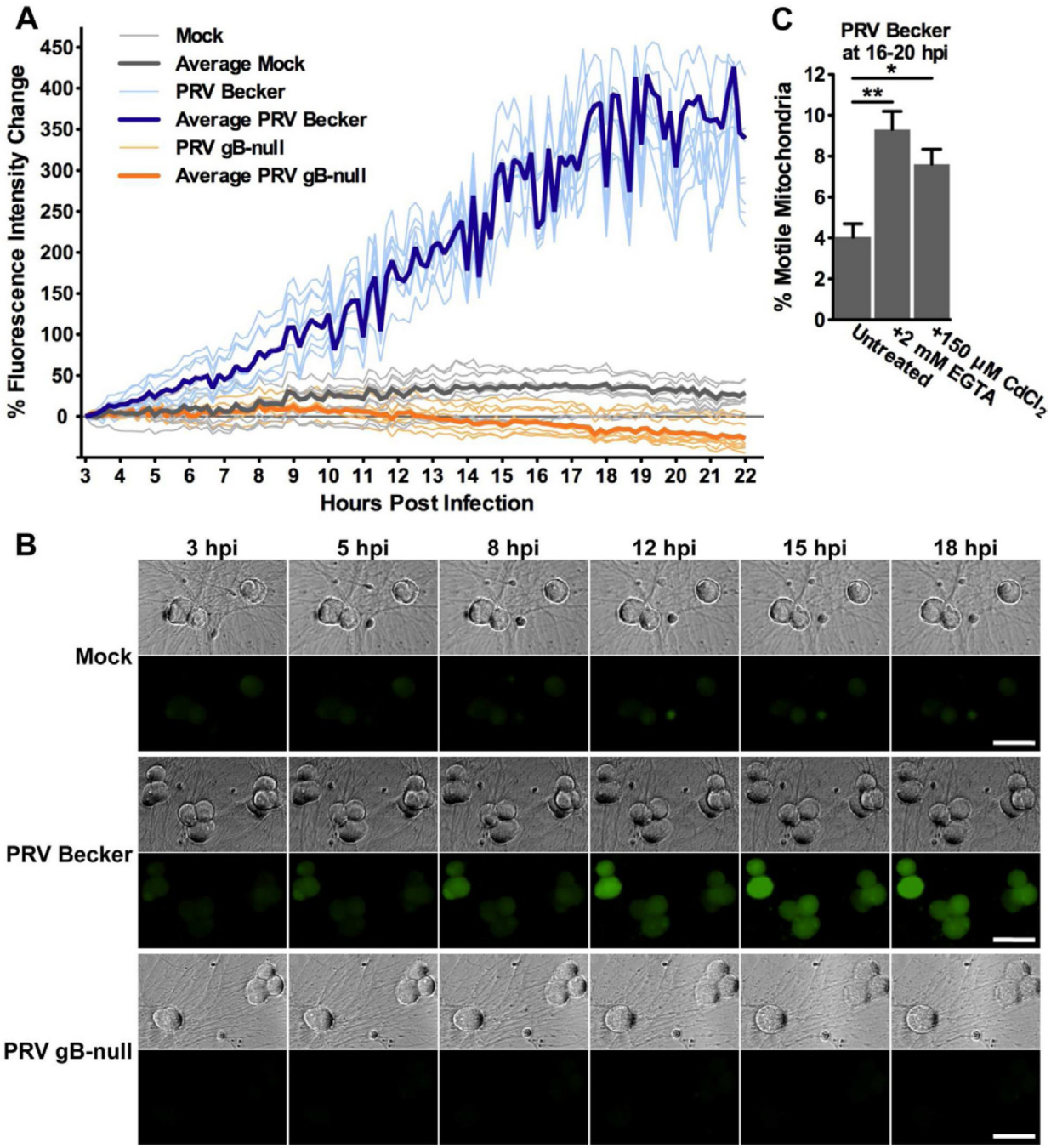

Figure 3. Intracellular [Ca^{2+}] increases during PRV infection in neurons and is dependent on gB-dependent membrane fusion

(A and B) Mock and infected neurons were stained with the Ca^{2+}-sensitive dye OGB-1. Neurons were imaged every 10 minutes between 3–22 hpi. (A) Change in fluorescence intensity for individual neuron cell bodies over the course of infection (following subtraction of background fluorescence intensity). Bolded lines represent the average change in fluorescence intensity for each condition, while light lines show trends for 8 individual representative neurons for each condition (total data is n=22 for mock, n=38 for PRV Becker, n=18 for PRV gB-null, acquired from neuron cell bodies in two fields of the same dish; additional biological replicates are presented in Figure S2A). (B) Representative

images of intracellular Ca^{2+} in mock and PRV infected neurons between 3–18 hpi. Phase contrast and OGB-1 staining (green) are shown (scale bar = 50 μm). (C) Quantification of the percentage of motile mitochondria in axons from PRV Becker infected SCG neurons at 16–20 hpi. Neurons were treated with 2mM EGTA (added at 0 hpi) or 150 μM $CdCl_2$ (added at 15 hpi). Error bars represent mean ± SEM. See also Figure S2 and Movie S2.

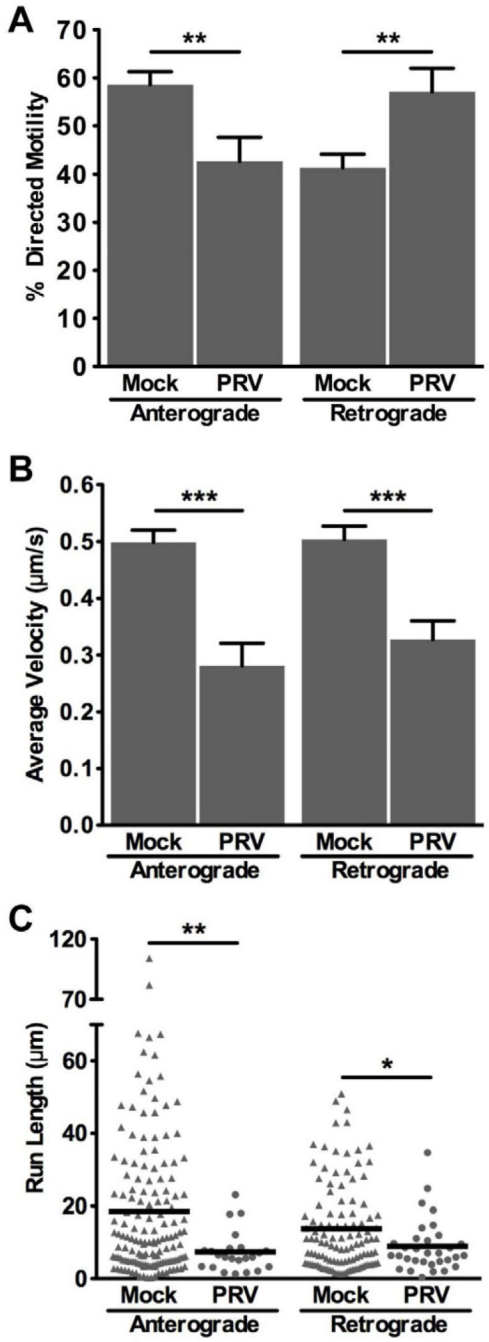

Figure 4. The small fraction of motile mitochondria in PRV infected axons has altered transport dynamics compared to mock infected

SCG neurons were grown in a modified system to assess the directionality of mitochondrial movement. Measurements were made from 10 axons for each condition from two biological replicates (n=243 mitochondria for mock and n=57 mitochondria for PRV Becker infected). Error bars represent mean ± SEM. (A) The percentage of mitochondria moving in the anterograde or retrograde directions. (B) The average velocity is defined as the weighted average velocity of all instantaneous velocities that contributed to a net movement in one direction and are not zero. (C) The run length is defined as the distance a mitochondrion

moved in one direction before stopping for more than two frames. Each symbol represents one measurement from mock (triangles) or PRV Becker infected (circles) axons.

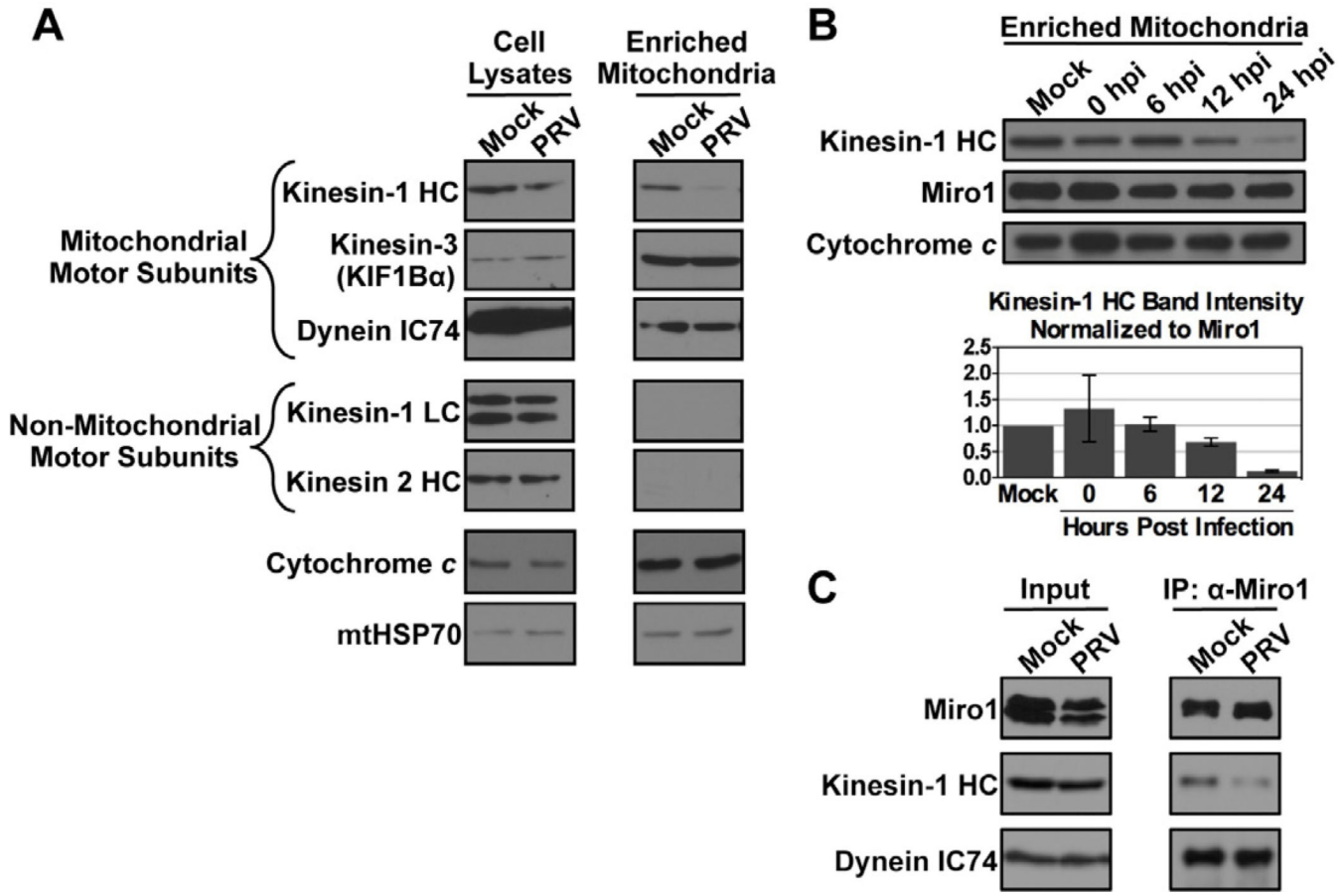

Figure 5. Western blot analysis of mitochondrial motor protein subunits during PRV infection

(A) Mitochondria were enriched from PC12 cells that were mock or PRV Becker infected at 18 hpi. Kinesin-1 heavy chain (HC), dynein intermediate chain IC74, and the kinesin-3 KIF1Bα are known mitochondrial motor protein subunits. Kinesin light chain (KLC) and kinesin-2 are non-mitochondrial motor protein subunits and serve as controls for the purity of the mitochondrial enrichment preparation. Cytochrome *c* and mitochondrial HSP70 (mtHSP70) are loading controls. (B) Mitochondria were enriched from mock or PRV infected PC12 cells at the indicated times post infection. At each time point, the levels of kinesin-1 HC were normalized to those of Miro1, which recruits kinesin-1 HC to the mitochondrial surface. The mean of two biological replicates is shown with bars representing the range. (C) Lysates of mock or PRV infected PC12 cells at 18 hpi were subjected to co-immunoprecipitation (IP) using anti-Miro1 antibodies. The input (left panels) and the precipitate (right panels) were probed using antibodies against Miro1, kinesin-1 HC, and dynein IC74.

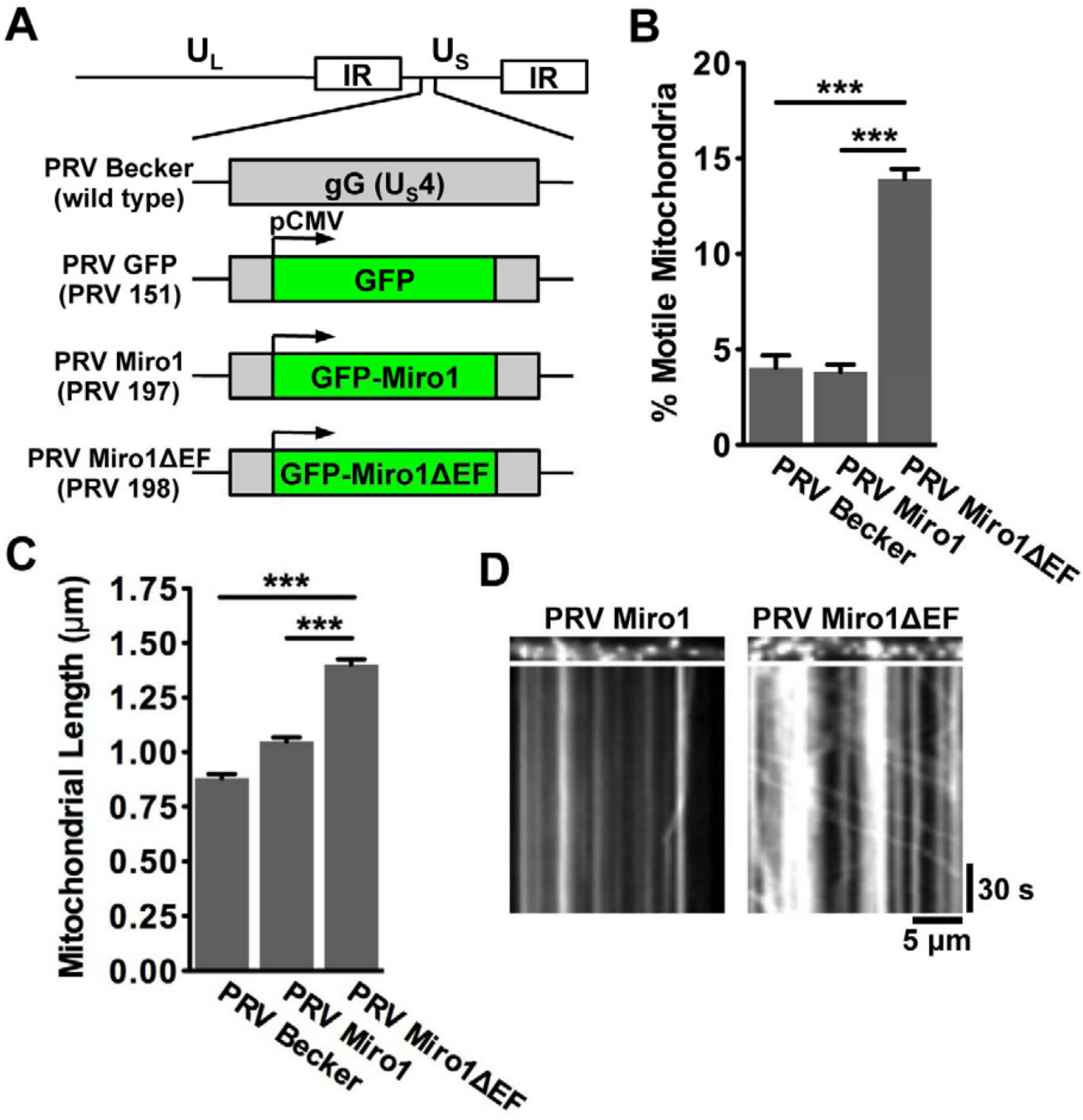

Figure 6. The Ca^{2+}-sensitive EF hand motifs of Miro1 are required for efficient disruption of mitochondrial dynamics during PRV infection

(A) Schematic representation of the genomes of PRV strains that express diffusible GFP (PRV 151; referred to as PRV GFP), GFP-Miro1 (PRV 197; referred to as PRV Miro), and GFP-Miro1ΔEF (PRV 198; referred to as PRV Miro1ΔEF). These proteins are expressed from the CMV promoter in the non-essential gG locus in the wild type PRV Becker background. (B) Quantification of the percentage of motile mitochondria in axons of neurons infected with PRV Becker, PRV Miro1, or PRV Miro1ΔEF at 12–16 hpi. (C) Quantification of mitochondrial lengths (n≥700 mitochondria per condition from six images that were acquired for each experimental condition from two biological replicates). Error

bars represent mean ± SEM. (D) Representative kymographs of mitochondria in SCG axons infected with PRV Miro1 and PRV Miro1ΔEF. See also Figure S3 and Movie S3.

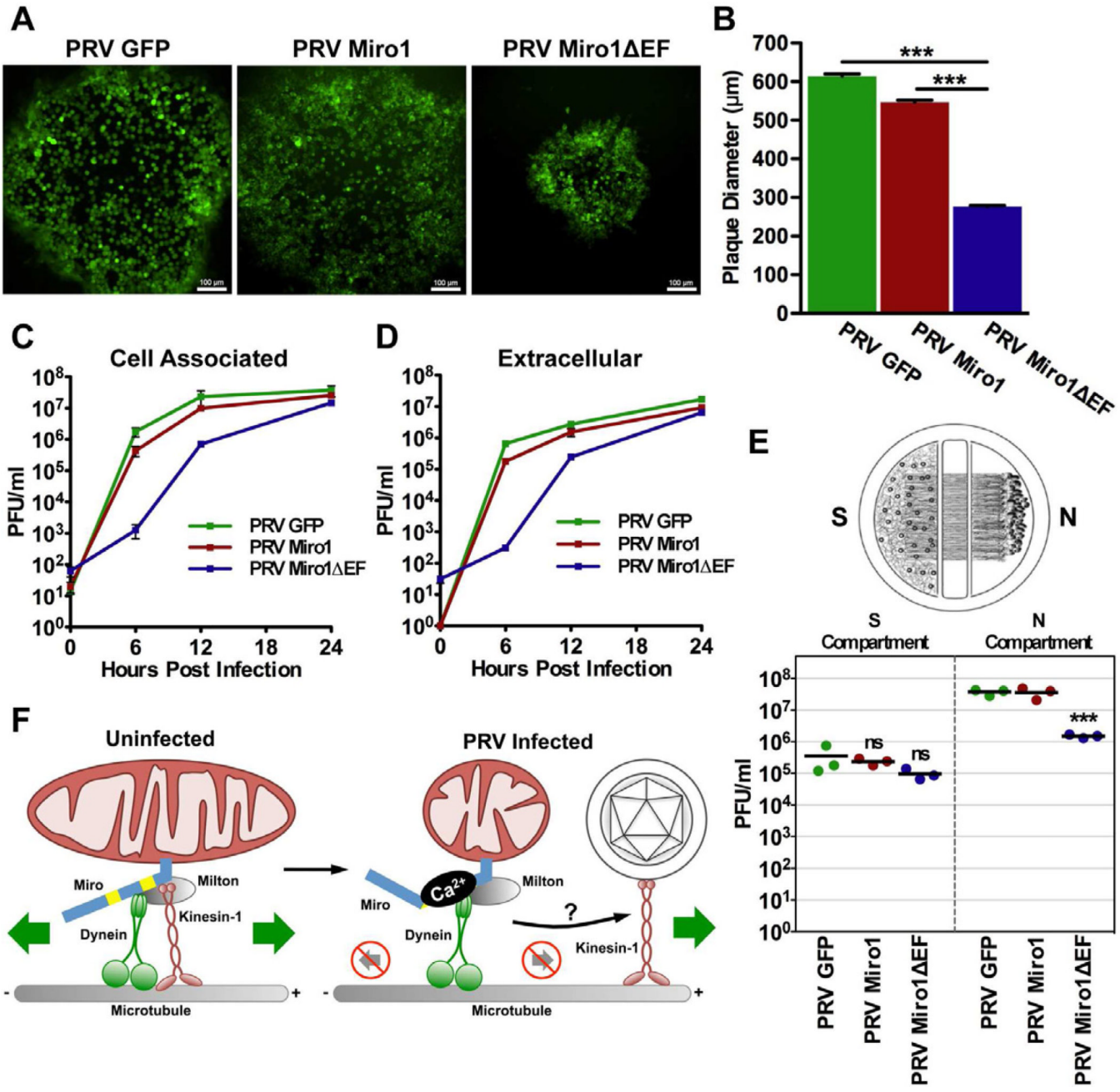

Figure 7. Disruption of mitochondrial motility through Ca^{2+}-sensitive Miro function is required for efficient growth and spread of PRV

(A) GFP-fluorescence of representative plaques from PRV GFP, PRV Miro1, and PRV Miro1ΔEF infected PK15 cells at 48 hpi (scale bars = 100 μm). (B) Quantification of plaque diameters at 48 hpi (n≥700 plaques per virus strain from two biological replicates). Error bars represent mean ± SEM. (C and D) Single step growth curve analysis of PRV GFP, PRV Miro1, and PRV Miro1ΔEF on PK15 cells (n=3 technical replicates per time point per virus strain). (E) Quantification of the efficiency of anterograde axonal spread using a chambered neuronal culture system. Cell bodies in the S compartment were infected at a high MOI with PRV GFP, PRV Miro1, or PRV Miro1ΔEF. Three chambers were used for each viral strain. At 24 hpi, the entire content of the S and N compartments were harvested separately and

titered on PK15 cells using a standard plaque assay. (F) Schematic model for the mechanism by which PRV infection alters mitochondrial motility and morphology.